Hindawi
Journal of Toxicology
Volume 2022, Article ID 7113958, 16 pages
https://doi.org/10.1155/2022/7113958

*Research Article*

# The Toxic Influence of Excess Free Iron on Red Blood Cells in the Biophysical Experiment: An In Vitro Study

**E. Kozlova**,[1,2,3] **E. Sherstyukova**,[1,2] **V. Sergunova**,[1] **A. Kozlov**,[2] **O. Gudkova**,[1] **V. Inozemtsev**,[1] **and A. Chernysh**[1]

[1]*Federal Research and Clinical Center of Intensive Care Medicine and Rehabilitology, V.A. Negovsky Research Institute of General Reanimatology, Moscow, Russia*
[2]*Sechenov First Moscow State Medical University (Sechenov University), Moscow, Russia*
[3]*Federal State Budget Educational Institution of Higher Education, M. V. Lomonosov Moscow State University (Lomonosov MSU), Faculty of Physics, Moscow, Russia*

Correspondence should be addressed to E. Sherstyukova; kmanchenko@yandex.ru

Received 10 November 2021; Accepted 10 January 2022; Published 26 February 2022

Academic Editor: You-Cheng Hseu



Iron is needed for life-essential processes, but free iron overload causes dangerous clinical consequences. The study of the role of red blood cells (RBCs) in the influence of excess free iron in the blood on the pathological consequences in an organism is relevant. Here, in a direct biophysical experiment *in vitro*, we studied the action of free iron overload on the packed red blood cell (pRBC) characteristics. In experiments, we incubated pRBCs with the ferrous sulfate solution ($Fe^{2+}$). We used free iron in a wide range of concentrations. High $Fe^{2+}$ concentrations made us possible to establish the pattern of the toxic effect of excess iron on pRBCs during a reduced incubation time in a biophysical experiment *in vitro*. It was found that excess free iron causes changes in pRBC morphology, the appearance of bridges between cells, and the formation of clots, increasing the membrane stiffness and methemoglobin concentration. We created a kinetic model of changes in the hemoglobin derivatives. The complex of simultaneous distortions of pRBCs established in our experiments can be taken into account when studying the mechanism of the toxic influence of excess free iron in the blood on pathological changes in an organism.

## 1. Introduction

Iron is a significant metal for various processes in biological systems, but there is no active mechanism for the excretion of excess iron from the body under conditions of iron overload (hemochromatosis) [1–3].

Overload of free iron in the blood has different origins: chronic iron overload is a common complication of repeated packed red blood cell (pRBC) transfusions [1, 4–6]; disorders of iron metabolism and chronic iron overload are observed in a number of acute and chronic inflammatory diseases and in acute respiratory distress syndrome [7, 8]; cell-free hemoglobin can become a source of excess free iron, arising under the action of hemolytic poisons [9], sickle cell anemia [10], hemodialysis [11], cardiac bypass [12], pulmonary arterial hypertension [13, 14], and sepsis [15–18], with phagocytosis of damaged RBCs [19, 20], hereditary hemochromatosis [21], and viral diseases [22–25], including SARS-CoV-2 [8, 26, 27]. Serious toxic effects were observed in a number of extreme cases [28–30].

Excess iron accumulation causes organ dysfunction [2, 4, 8, 31–36]. Iron overload is especially dangerous for critically ill patients [37–39]. Often, pathological consequences are associated with the action of various factors on elements and processes in the blood in the cardiovascular system: the coagulation system is changed, blood clotting, hemostasis, and thrombosis that is clinically significant are arisen [31, 40, 41].

In these cases, RBCs are the key elements. Therefore, we raised a question what is happening or can potentially happen in RBCs under toxic influence of free blood iron. The changes in RBC morphology after influence of iron on them

are shown in a number of scientific articles. There are studies that have established a change in the morphology of RBCs *in vitro* as a result of the action of free iron ions in high concentrations. The shape change was observed in the blood of people with hemochromatosis [36, 42].

As a rule, RBC shape distortion and an increase in their membrane stiffness are associated with the acceleration of oxidative processes under the action of physical and chemical factors [43–46].

Free iron is potentially extremely toxic due to its ability to generate reactive oxygen species (ROS), which are involved in various redox processes [9, 31, 47–49]. One of the consequences and at the same time a biomarker of the development of oxidative processes in the blood is the formation of methemoglobin (MetHb) [50, 51].

In this work, we conducted direct biophysical experiments to solve the problem of revealing and quantitative estimation of toxic effects of free iron on pRBCs in an *in vitro* model. We used free iron in a wide range of concentrations. High $Fe^{2+}$ concentrations made us possible to establish the pattern of the toxic effect of excess iron on pRBCs during a reduced incubation time in a biophysical experiment *in vitro*. For quantitative registration of pRBC modifications, we used atomic force microscopy (AFM). Atomic force spectroscopy (AFS) allowed us to measure the local Young's modulus of native membranes. High-resolution digital spectroscopy and the nonlinear curve fitting method for the analysis of optical spectra allowed us to experimentally establish the kinetics of MetHb formation under the influence of excess $Fe^{2+}$. We created a mathematical kinetic model of changes in the concentrations of $Fe^{2+}$ and hemoglobin derivative concentrations, which adequately describes the experimental data and allows to estimate the rate constants of redox processes.

## 2. Materials and Methods

*2.1. Blood Products.* Packed red blood cells were obtained from the clinical centers of blood transfusion in Moscow, Russian Federation. All of the experiments were conducted in accordance with guidelines and regulations of the Federal Research and Clinical Center of Intensive Care Medicine and Rehabilitology, V.A. Negovsky Scientific Research Institute of General Reanimatology, Moscow, Russian Federation. All of the experimental protocols were approved by this institute.

A total of 5 bags with pRBCs were used in the study. pRBC units were prepared from the whole blood (450 ml ± 10%) by removing the plasma fraction after centrifugation. Leukocyte-depleted pRBCs in airtight bags were stored with standard CPD anticoagulant (63 ml) (citrate, phosphate, and dextrose) and SAGM additive solution (100 ml) (saline, adenine, glucose, and mannitol) at a temperature of +4°C. The hematocrit of the pRBCs was 60–65%. Samples of pRBCs for *in vitro* experiments were withdrawn on days 3–5.

Stages of the study are shown in detail in Figure 1.

*2.2. Preparation of Ferrous Sulfate Solution.* A ferrous sulfate stock solution (solution A) was prepared by dissolving 20 mg iron (II) sulfate heptahydrate ($FeSO_4{\cdot}7H_2O_2$) (Sigma-Aldrich, USA) with 1.0ml of PBS (pH 7.4)/distilled water, $C_{Fe^{2+}} = 71.9$ mM. Then, 100 $\mu$l of solution A were added to 4 ml of distilled water/PBS (solution B). The initial concentration of $Fe^{2+}$ in lysate/suspension was 1700 $\mu$M, and this is designated as $Fe^{2+}1700$. To study the influence of $Fe^{2+}$ in initial various concentrations, we changed solution A to receive $C_{Fe^{2+}}$ from 212.5 to 13600 $\mu$M. We used free iron in a wide range of concentrations $C_{Fe^{2+}}$.

High $Fe^{2+}$ concentrations make it possible to establish the pattern of the toxic effect of excess iron on pRBCs during a reduced incubation time in a biophysical experiment *in vitro*.

*2.3. pRBC Lysate and Suspension Preparation In Vitro.* To prepare the lysate and suspension of pRBCs *in vitro*, the components of the solution in which the pRBCs were stored were removed. To do this, 200 $\mu$l of pRBCs was washed in 1 ml of phosphate buffer saline (PBS) at pH 7.4 (MP Biomedicals, France). This suspension was centrifuged at 2,000 rpm for 5 minutes in a Universal 320 centrifuge (Andreas Hettich GmbH & Co. KG, Germany). This procedure was carried out twice. Then, the lysate (L) was prepared by mixing 15 $\mu$l of pRBCs and 100 $\mu$l of distilled water, and the pRBC suspension (S) was prepared by mixing 15 $\mu$l of pRBCs and 100 $\mu$l of PBS. Then, 100 $\mu$l of lysate/suspension were diluted in 4.1 ml of solution B. The time of iron interaction with pRBCs was named as the incubation time and designated as $t_{inc}$. Stages of the experiment are shown in Figures 1(b) and 1(c).

*2.4. Spectrophotometry.* For the spectrophotometry study, 100 $\mu$l of lysate was diluted in 4 ml of distilled water, or 100 $\mu$l of suspension was diluted in 4 ml of PBS with 100 $\mu$l solution A as shown in Figures 1(b) and 1(c). The working solution with ferrous sulfate and lysate was designated as $LFe^{2+}$ 1700, and the similar suspension solution was designated as $SFe^{2+}1700$; the solution without ferrous sulfate for lysate was designated as $LFe^{2+}$ 0, and the suspension was designated as $SFe^{2+}$ 0. The incubation times of the lysate of pRBCs were 0, 15, 30, 45, 60, 90, 120 min, and 24 hours, and for the suspension of pRBCs, the incubation times were 1, 5, and 24 hours.

To determine the concentration of hemoglobin derivatives, the optical absorption spectra were measured using a Unico 2800 digital spectrophotometer (United Products & Instruments, USA). The experimental spectrum $D(\lambda)_{exp}$ was measured in the wavelength range of 500–700 nm with steps of 0.5 nm. The concentrations of hemoglobin derivatives ($HbO_2$, Hb, and MetHb) were measured according to their individual absorptivities at different wavelengths using the nonlinear curve fitting method of experimental spectra.

*2.5. Nonlinear Curve Fitting Optical Spectra.* For the determination of hemoglobin derivatives, the nonlinear curve fitting method was used as described in [52, 53]. Briefly, it is necessary to experimentally obtain the set of optical densities measured at corresponding wavelengths $D_l(\lambda_l)_{exper}$, where $l$

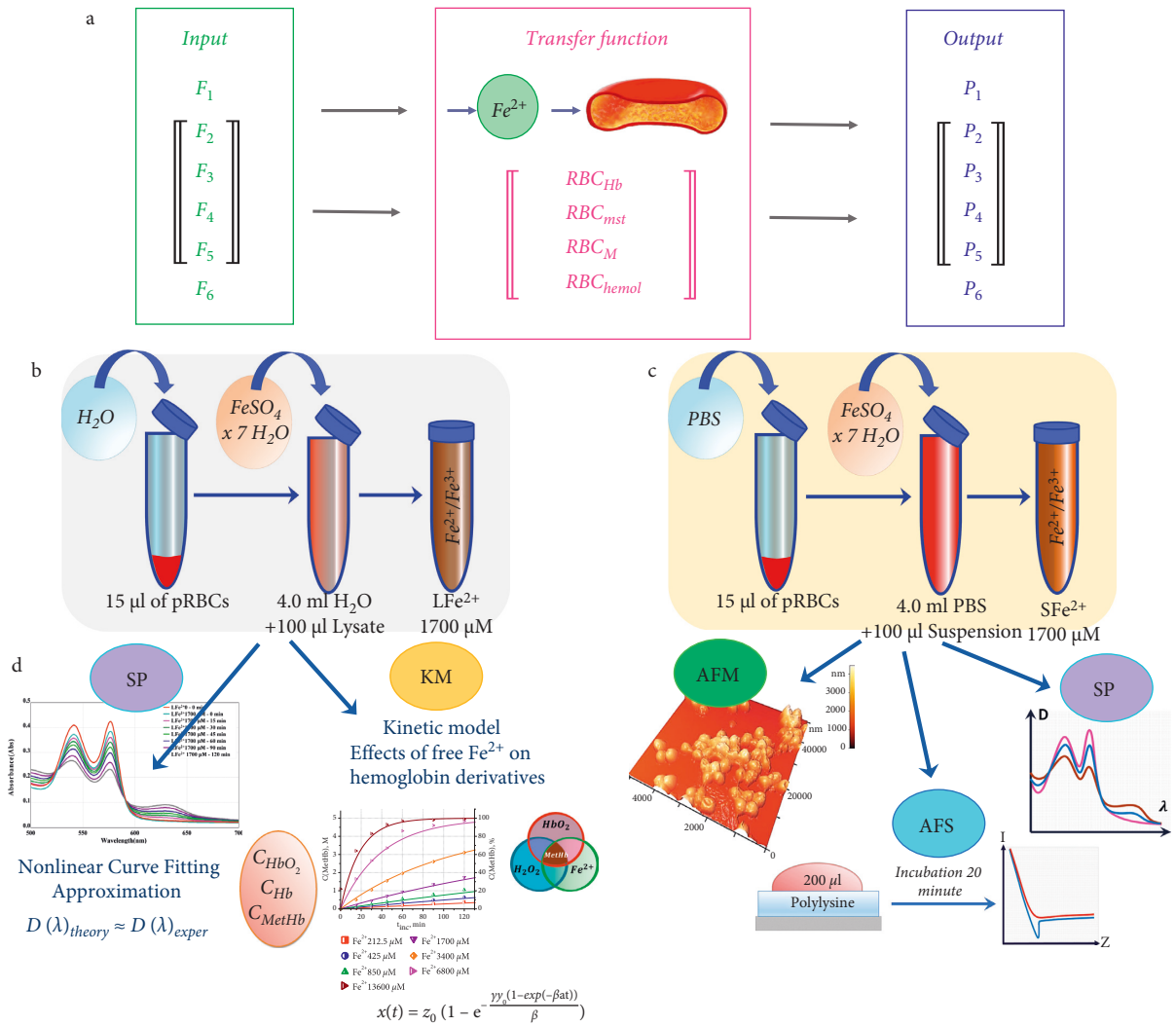


Figure 1: RBCs as a transfer link in the influence of factors determining an excess of $Fe^{2+}$ on clinical consequences in organisms. (a) A schematic representation of the influence of various factors determining excess $Fe^{2+}$ on clinical consequences in the organism. Input includes $F_i$: factors determining excess $Fe^{2+}$; transfer function includes pathological changes in RBCs: $RBC_{Hb}$, content of hemoglobin derivatives; $RBC_{mst}$, membrane stiffness; $RBC_M$, cell morphology; $RBC_{hemol}$, hemolysis; output includes $P_i$: pathological clinical consequences. (b) Experimental design for pRBC lysate. The designation of pRBC lysate with iron is $LFe^{2+}$ 1700. (c) Experimental design for pRBC suspension. The designation of pRBC suspension with iron is $SFe^{2+}$ 1700. (d) Methods to study the action of excess $Fe^{2+}$ on RBCs. AFM, atomic force microscopy; AFS, atomic force spectroscopy; KM, kinetic model; SP, spectrophotometry.

is the number of wavelengths and $\lambda_l$ is the set of wavelengths. Then, we define our own function $D_l(\lambda_l)_{\text{theor}}$ by using Origin's flexible Fitting Function Builder by Origin Pro 2019 (OriginLab Corporation, USA):

$$D_l(\lambda_l)_{\text{theor}} = \varepsilon_{\text{HbO}_2,l} C_{\text{HbO}_2} L + \varepsilon_{\text{Hb},l} C_{\text{Hb}} L + \varepsilon_{\text{MetHb},l} C_{\text{MetHb}} L + K + \frac{S}{\lambda_l^4}. \quad (1)$$

In this equation, there are known values: molar absorptivity coefficients at given wavelengths $\lambda_l$ ($\varepsilon_{\text{HbO}_2,l}$, $\varepsilon_{\text{Hb},l}$, and $\varepsilon_{\text{MetHb},l}$) [50] and the thickness of the layer $L$. There are also unknown values: concentrations of corresponding hemoglobin derivatives ($C_{\text{HbO}_2}$, $C_{\text{Hb}}$, and $C_{\text{MetHb}}$) and coefficients of scattering ($K$ and $S$). These parameters must be determined by fitting the model.

This function is created according to biophysical considerations. Because red blood cells are studied in PBS, it is necessary to consider not only the absorption but also the scattering processes. The intensity of these processes will be different for various wavelengths.

The coefficient $K$ describes the scattering of light on pRBCs when the wavelength is smaller than the diameter of pRBCs, $\lambda \ll d$. The coefficient $S$ corresponds to Rayleigh scattering when the scattering particles are very small, $\lambda \gg d'$. In the nonlinear curve fitting model, the experimental optical density data $(D_l(\lambda_l)_{\text{exper}})$ are used instead of $D_l(\lambda_l)_{\text{theor}}$. Computing the fitted values in nonlinear regression is an iterative procedure performed using the Levenberg–Marquardt algorithm. Iteration to adjust parameter values continues to make data points closer to the theoretical curve. The adjusted R-squared is the measure of the goodness of fit.

The concentration of total hemoglobin $C_{\text{total}}$ is the sum of hemoglobin derivative concentrations, in *mmol/l*. The percentage of each derivative in pRBCs is the ratio, particularly,

$$C_{\text{MetHb}}\% = 100\frac{C_{\text{MetHb}}}{C_{\text{total}}}\%. \quad (2)$$

*2.6. Kinetic Model of Change of Hemoglobin Derivative Concentrations under the Influence of $Fe^{2+}$.* The mathematical modeling was used to study the dynamics of the increase in the concentration of MetHb under the actions of ferrous sulfate solution in different concentrations. The kinetics of the $Fe^{2+}$ and $H_2O_2$ interaction as well as the kinetics of an increase in the concentration of MetHb are analyzed. Based on the law of mass action, ordinary differential equations describing the kinetics of chemical reactions were recorded. The kinetic equations were solved using the method of separation of variables, taking into account the initial conditions. Details of the model are given in the text.

The obtained theoretical dependence $C_{\text{MetHb theor}}(t)$ was used as the basis for the approximation of the experimental data $C_{\text{MetHb exper}}(t)$. As a result, the unknown parameters of the approximation were estimated—the rate constants of the reactions and the concentration of $H_2O_2$.

*2.7. Atomic Force Microscopy.* To obtain images of cells, a smear of pRBC was formed. First, 4.2 ml of pRBC suspension ($SFe^{2+}0$ and $SFe^{2+}1700$) was sedimented by centrifugation at 2,000 rpm for 5 minutes. Next, 50 $\mu$l of 1% glutaraldehyde solution (Panreac Quimica S.L.U., Spain) was added to 50 $\mu$l of sediment for 4 minutes. To wash the cells, 500 $\mu$l of distilled water was added to the pRBC suspension. After centrifugation at 2,000 rpm for 5 minutes, the supernatant was removed and 300 $\mu$l of distilled water was added. Then, the sample was centrifuged again, and the supernatant was removed. The smear of sediment was prepared using V-sampler (Vision, Austria).

For the analysis of cell morphology, an NTEGRA Prima atomic force microscope (NT-MDT Spectrum Instruments, Russian Federation) was used. Scanning was carried out in semicontact mode with the NSG01 probe (probe radius 10 nm, resonance frequency 87–230 kHz, and force constant 1–15 N/m) (TipsNano, Estonia). During scanning, fields with sizes of $50 \times 50\,\mu m^2$, $30 \times 30\,\mu m^2$, and $10 \times 10\,\mu m^2$ were selected. The number of dots per line was 1024. The characteristic incubation times for pRBC samples were 1, 5, and 24 hours. Various concentrations of ferrous sulfate were studied. For each incubation time and concentration of ferrous sulfate, images and their profiles were obtained, which made it possible to estimate the spatial characteristics: $L$ is the spatial period between the minima of the structure, and $h$ is the average height from the concaves to the maxima. The SPM Nova software (NT-MDT Spectrum Instruments, Russian Federation) was used to record AFM images.

*2.8. Atomic Force Spectroscopy.* The stiffness of pRBC membranes is characterized by Young's modulus (E). The method of sedimentation was used to prepare the sample. To do this, 300 $\mu$l of pRBC suspension ($SFe^{2+}1700$ and $SFe^{2+}0$) was applied to glass coverslips coated in poly-L-lysine hydrobromide (MP Biomedicals, France) and was left for 30 minutes for adhesion. Then, the coverslips were washed in PBS. For this, the type of cantilever SD-R150-T3L450B-10 (Nanosensors, Switzerland) was used (probe radius 150 nm, resonance frequency 21 kHz, force constant 1 N/m). Force curves were measured only on native cells, without adding chemical fixatives. Measurements were carried out after 1 and 24 hours.

*2.9. Statistical Analysis.* For each bag, 3 smears of pRBCs were prepared. On each smear, 3 fields of $50 \times 50\,\mu m^2$ were scanned. For one bag, morphology analysis was carried out for an average of 500 cells. In total, approximately 2500 cells were studied. For each bag, 100 force curves were measured for one sample. A total of 2000 pRBCs were analyzed in the study. For each blood sample for spectrophotometry, the experiments were performed three times.

Statistical processing was performed using the Origin Pro 2019 software. All data are presented as the mean ± SD, and replicate information is indicated in the figure legends. The normality Shapiro–Wilk test for all data was used. The one-way ANOVA test followed by the Tukey's post hoc test for experimental data comparison was used. Pearson correlation analyses were performed to determine the close relationships between MetHb level, hemolysis level, and the average number of discocytes on a smear.

## 3. Results and Discussion

*3.1. RBCs as a Possible Key Link in the Adverse Effect of Excess Free Iron.* Various primary factors $F_i$ (frequent blood transfusion $F_1$, hereditary hemochromatosis $F_2$, severe blood loss $F_3$, bacteria and viruses $F_4$, sepsis $F_5$, and chemical pharmaceuticals $F_6$) results in free iron overload ($Fe^{2+}$) in the blood leading to pathological consequences in the organism $P_i$ (organ dysfunction $P_1$, atherosclerosis $P_2$, microvascular pulmonary thrombovasculitis obliterans (in particular, with COVID-19) $P_3$, carcinogenesis $P_4$, intravascular hemolysis $P_5$, and diabetes $P_6$). In the chain of these events, RBCs play a key role as the transfer function between the primary factors and the pathological consequences $P_i$, $F_i \longrightarrow \text{RBCs} \longrightarrow P_i$ (Figure 1(a)).

In this study, we consider the potential distortions of excess $Fe^{2+}$ action on RBCs, shown in red in Figure 1(a). In particular, changes in the content of hemoglobin derivatives ($RBC_{\text{Hb}}$), and changes in cell morphology ($RBC_M$), hemolysis ($RBC_{\text{hemol}}$), and membrane stiffness ($RBC_{\text{mst}}$), arising simultaneously under the influence of excess $Fe^{2+}$ are considered.

We investigated the impact of free $Fe^{2+}$ on the pRBC suspension and lysate (Figure 1(b) and 1(c)) *in vitro* and identified disruption in cell elements. In the experiments, dissolved $FeSO_4$ was added to the test sample (Figure 1(b) and

1(c)). Analysis was performed using digital spectrophotometry ($\Delta\lambda = 0.5$ nm), AFM (resolution limit of 0.1 nm in height and 10 nm in length), AFS, and mathematical modeling (Figure 1(d)). More details about the *in vitro* systems are indicated in Materials and Methods.

*3.2. Nonlinear Kinetics of MetHb Formation Was Registered with Excessive Content of Free $Fe^{2+}$.* The absorption spectrum of pRBC lysates after the addition of $FeSO_4$ salt solution changes significantly over time (Figure 2(a)). When the pRBC lysate is incubated with free iron, the absorption peak at $\lambda_3 = 630$ nm appears and grows, so the process of conversion of oxyhemoglobin $HbO_2$ to MetHb develops. For $Fe^{2+}$ of 1700 $\mu$M during a 60 min incubation, the MetHb content developed almost linearly (Figure 2(b)). After 60 minutes, nonlinear kinetics of the MetHb increase in the pRBC lysate was observed (Figure 2(b)). The instantaneous rate of MetHb formation can be calculated as $V_{\mathrm{MetHb}}(t) = (\mathrm{d}C_{\mathrm{MetHb}}(t)/\mathrm{d}t) = tg\alpha$; accordingly, by time $t$, its content will be $C_{\mathrm{MetHb}}(t) = \int_0^t V_{MetHb}(t)\mathrm{d}t$.

Three hemoglobin derivatives play important roles in the absorption process: $HbO_2$, Hb, and MetHb. The nonlinear curve fitting method was used to estimate unknown concentrations of the hemoglobin derivatives $C_{\mathrm{HbO_2}}$, $C_{\mathrm{Hb}}$, and $C_{\mathrm{MetHb}}$, which best described the experimental data (Figure 2(a)). For this, the optical spectrum $D_l(\lambda_l)_{\mathrm{exper}}$ was approximated by the theoretical curve $D_l(\lambda_l)_{\mathrm{theor}}$, according to which for each wavelength $\lambda_l$ optical density is a sum of products of the molar absorption coefficient ($\varepsilon_{\mathrm{HbO_2},l}$, $\varepsilon_{\mathrm{Hb},l}$, and $\varepsilon_{\mathrm{MetHb},l}$) and concentrations $C_i$ for the corresponding hemoglobin derivatives (Equation (1)). Equation (1) was used earlier in our studies [52–54].

Figure 2(c) shows the measured spectra $D_l(\lambda_l)_{\mathrm{exper}}$ and fitting curves $D_l(\lambda_l)_{\mathrm{theor}}$, plotted for the parameter $C_i$, calculated by equation (1), to determine the effect of $Fe^{2+}$ 1700 $\mu$M on the pRBC lysate with incubation times of 0, 30, 60, and 120 min. For the pRBC lysate, the calculated scattering coefficients $K$ and $S$ (equation (1)) equaled zero.

Free $Fe^{2+}$ exposure at different concentrations $C_{\mathrm{Fe^{2+}}}$ led to increasing of $C_{\mathrm{MetHb}}(t)$. Moreover, the rate of $C_{\mathrm{MetHb}}(t)$ growth increased with the increment of the initial concentration of $Fe^2$ (Figure 2(d)). Experimental data for incubation times up to 120 min are shown a larger scale in Figure 2(e). In the first 15 min, the initial rates of MetHb formation were $V_{\mathrm{MetHb}}(t) = tg\alpha = 0.04\%, 0.13\%, 0.27\%$, and 2.2% for $Fe^{2+}$ 212.5, 850, 1700, and 6800 $\mu$M, correspondingly.

The steady state level of the $C_{\mathrm{MetHb\,stst}}$ and the time to reach it $t_{\mathrm{MetHb\,stst}}$ (Figures 2(d)–2(f)) depended on the concentration $C_{\mathrm{Fe^{2+}}}$. Therefore, with $C_{\mathrm{Fe^{2+}}} = 6800$–$13600$ $\mu$M, $C_{\mathrm{MetHb\,stst}} = 97 - 100\%$ and $t_{\mathrm{MetHb\,stst}} = 100 - 200$ min. At lower concentrations, $C_{\mathrm{Fe^{2+}}} = 212.5$–$425$ $\mu$M, $C_{\mathrm{MetHb\,stst}} = 38 - 60\%$, and $t_{\mathrm{MetHb\,stst}} > 1200 - 1400$ min. Up to $Fe^{2+}$ 6800 $\mu$M, the dependence of $C_{\mathrm{MetHb}}(C_{\mathrm{Fe^{2+}}})$ was linear for pRBC lysate incubation times up to 60 min (Figure 2(f)).

The formation of MetHb in cells under the influence of $Fe^{2+}$ on the pRBC suspension occurred 5–10 times slower than in the lysate (Figures 2 and 3).

*3.3. Excess Free Iron Results in pRBC Polymorphism.* The result of the interaction of $Fe^{2+}$ and $H_2O_2$ is the formation of a highly reactive radical $OH^{\cdot}$, which attacks lipids and proteins in RBC membranes. It is known that, as a result of the violation of ionic equilibrium during the development of oxidative processes under the action of various physical and chemical factors, cell cytoskeleton and membrane nanosurface changes [46, 55–58], resulting in RBC morphology alterations [45, 56, 58, 59].

In this study, we investigated how MetHb formation was accompanied by changes in pRBC morphology under $Fe^{2+}$ influence (Figure 3). AFM images of typical fragments ($40 \times 40$ $\mu m^2$) of conventional RBC smears are shown in Figure 3. For comparison, controls (pRBC shapes and spectra without $Fe^{2+}$ exposure) are shown in Figure 3. MetHb levels were $0.5 \pm 0.5\%$ ($0.025 \pm 0.025$ $\mu$M) for $t_{\mathrm{inc}} = 1$ hour, $1.5 \pm 0.5\%$ ($0.075 \pm 0.025$ $\mu$M) for $t_{\mathrm{inc}} = 5$ hours, and $5 \pm 1\%$ ($0.25 \pm 0.05$ $\mu$M) for $t_{\mathrm{inc}} = 24$ hours, while the levels of hemolysis were $0.5 \pm 0.5\%$, $1.0 \pm 0.5\%$, and $10 \pm 1\%$, respectively (Figures 3(a)–3(c)). After the influence of $Fe^{2+}$1700 $\mu$M on pRBC suspension, the MetHb level and hemolysis did not differ from the control values for $t_{\mathrm{inc}} = 1$ hour, almost increasing to $20 \pm 2\%$ ($1.0 \pm 0.1$ $\mu$M) for $t_{\mathrm{inc}} = 5$ hours and up to $82 \pm 3\%$ ($4.10 \pm 0.15$ $\mu$M) for $t_{\mathrm{inc}} = 24$ hours, while the levels of hemolysis were $21 \pm 3\%$ and $58 \pm 5\%$, respectively. A close correlation was established between the mean values of the MetHb level and the level of hemolysis, $r_{\mathrm{MetHb-Hemolysis}} = 0.98$.

The formation of MetHb was accompanied by a significant change in cell forms (Figures 3 and 4). In the control sample, two types of cells were observed (Figure 4(b)): discocytes and echinocytes (approximately 3% at $t_{\mathrm{inc}} = 5$ hours and approximately 14% at $t_{\mathrm{inc}} = 24$ hours). After exposure to $Fe^{2+}$1700 $\mu$M at $t_{\mathrm{inc}} = 1$ hour, the morphology of the cells changed insignificantly, and after $t_{\mathrm{inc}} = 5$ hours, significant changes had already occurred. Four types of cells were observed (Figure 4(c)): $76 \pm 4\%$ were spherocytes and microspherocytes (approximately half), $18 \pm 4\%$ became ghosts, and only $6 \pm 1\%$ remained discocytes. After $t_{\mathrm{inc}} = 24$ hours, $60 \pm 4\%$ of the cells became ghosts and $34 \pm 2\%$ were microspherocytes. There were small number of discocytes (1%) and spherocytes (5%).

Thus, the most part of the cells hemolyzed and became ghosts. We experimentally established that pRBC damage in result of $Fe^{2+}$ exposure occurs through two mechanisms: (1) swelling of cells, the formation of spherocytes, and ultimately their hemolysis and formation of ghosts and (2) the formation of microspherocytes. These forms are irreversible and their formation, even in small amounts, can significantly reduce the quality of pRBCs and their functional ability. The effects of altering the pRBC morphology were enhanced with increasing concentrations of free $Fe^{2+}$ in suspension (Figure 4(d)). An inverse correlation was established between the mean MetHb level and the mean number of discocytes on a smear $r_{\mathrm{MetHb-Discocyte}} = -0.72$.

We identified pRBC ghosts in AFM images, and accordingly, decreases in the level of optical density in the optical spectra were fixed (Figure 4). There was a good

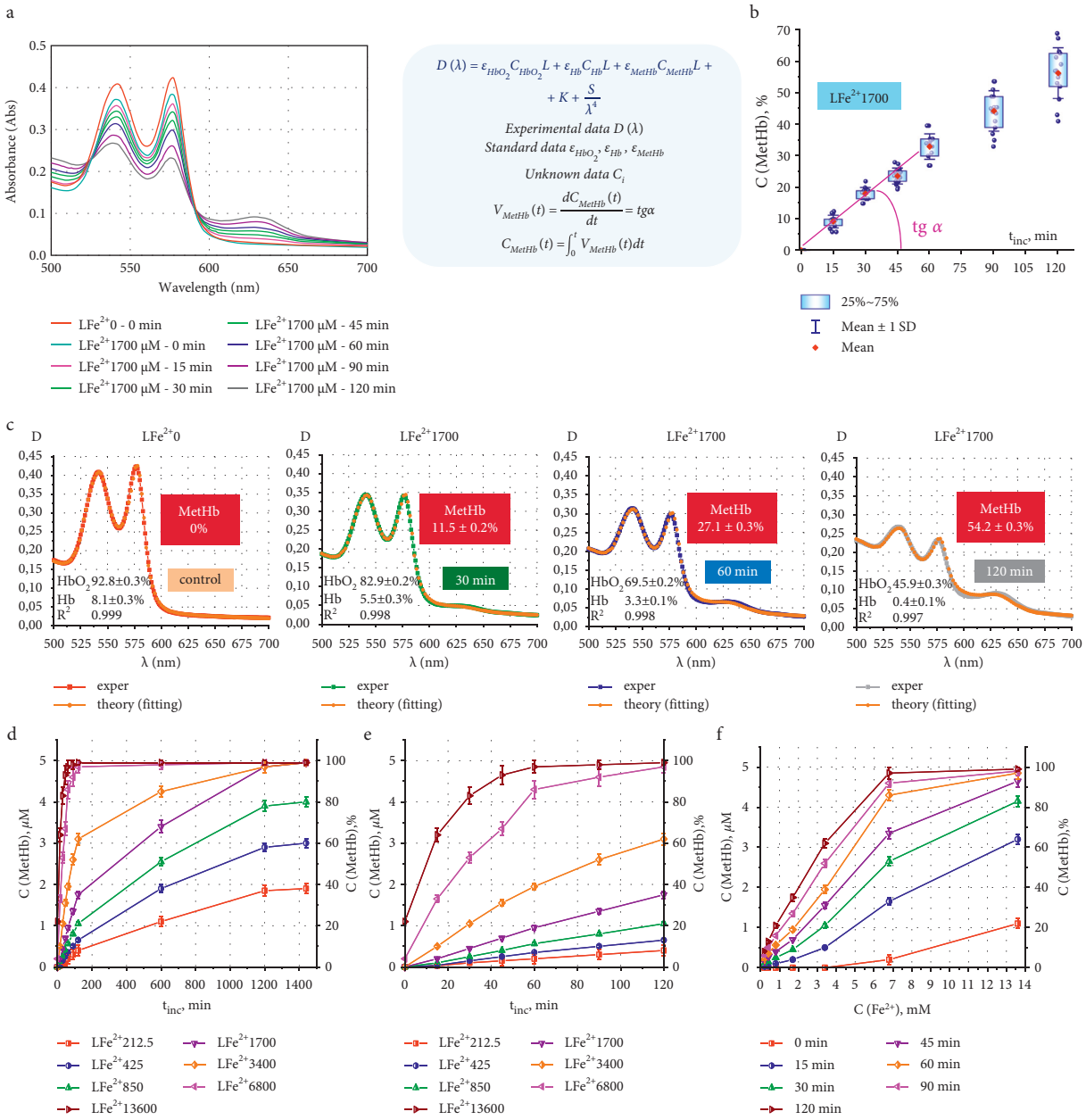


FIGURE 2: Increasing MetHb content with excessive content of free $Fe^{2+}$. (a) Optical spectra of the $LFe^{2+}$ 1700 sample, incubation time $t_{inc} = 0$, 15, 30, 45, 60, 90, and 120 minutes. On the right are the equations for calculating the concentrations of hemoglobin derivatives. (b) Increase in $C_{MetHb}(t)$ depending on the incubation time for the $LFe^{2+}$ 1700 sample. Data are presented as box chart, from the 25th to the 75th percentile, whiskers are presented as mean ± SD, and the red square denotes mean. Dots are the experimental data. (c) Fitting results of the experimental data for the $LFe^{2+}$ 0 and $LFe^{2+}$ 1700 samples ($t_{inc} = 0$, 30, 60, and 120 min). Concentrations of hemoglobin derivatives are shown on each graph and were calculated by the nonlinear curve fitting method. Additionally, the R-square parameter is shown. (d, e) Dynamics of changes in the $C_{MetHb}(t)$ for different initial concentrations of free $Fe^{2+}$ in dependence of time (0–1500 min (d) and 0–120 min (e)); on the graph axes, MetHb concentrations are in μM from the left and in % from the right. Initial concentrations of free $Fe^{2+}$ are shown in different colors. (f) Increase in the $C_{MetHb}(t)$ as a function of the initial free $Fe^{2+}$ concentration. Different colors correspond to different incubation times.

correlation of the percentage of ghosts on AFM images with the number of hemolyzed cells measured by the residual level in the absorption spectrum of the pRBC suspension: ghosts 18 ± 4% and hemolysis level 21 ± 3% after 5 hours of incubation, and ghosts 60 ± 4% and hemolysis level 58 ± 5% after 24 hours of incubation; thus, $r_{\text{Hemolysis–Ghost}} = 0.99$.

*3.4. Bridges, Chains, and Clots of pRBCs Were Formed.* In experiments, there were the self-organization of pRBCs. Connections between cells arose in the form of bridges, and chains were formed; as a result, they were combined into conglomerates and clots (Figure 5(a)). The height of the bridges between the cells ranged from 300 to 600 nm, the

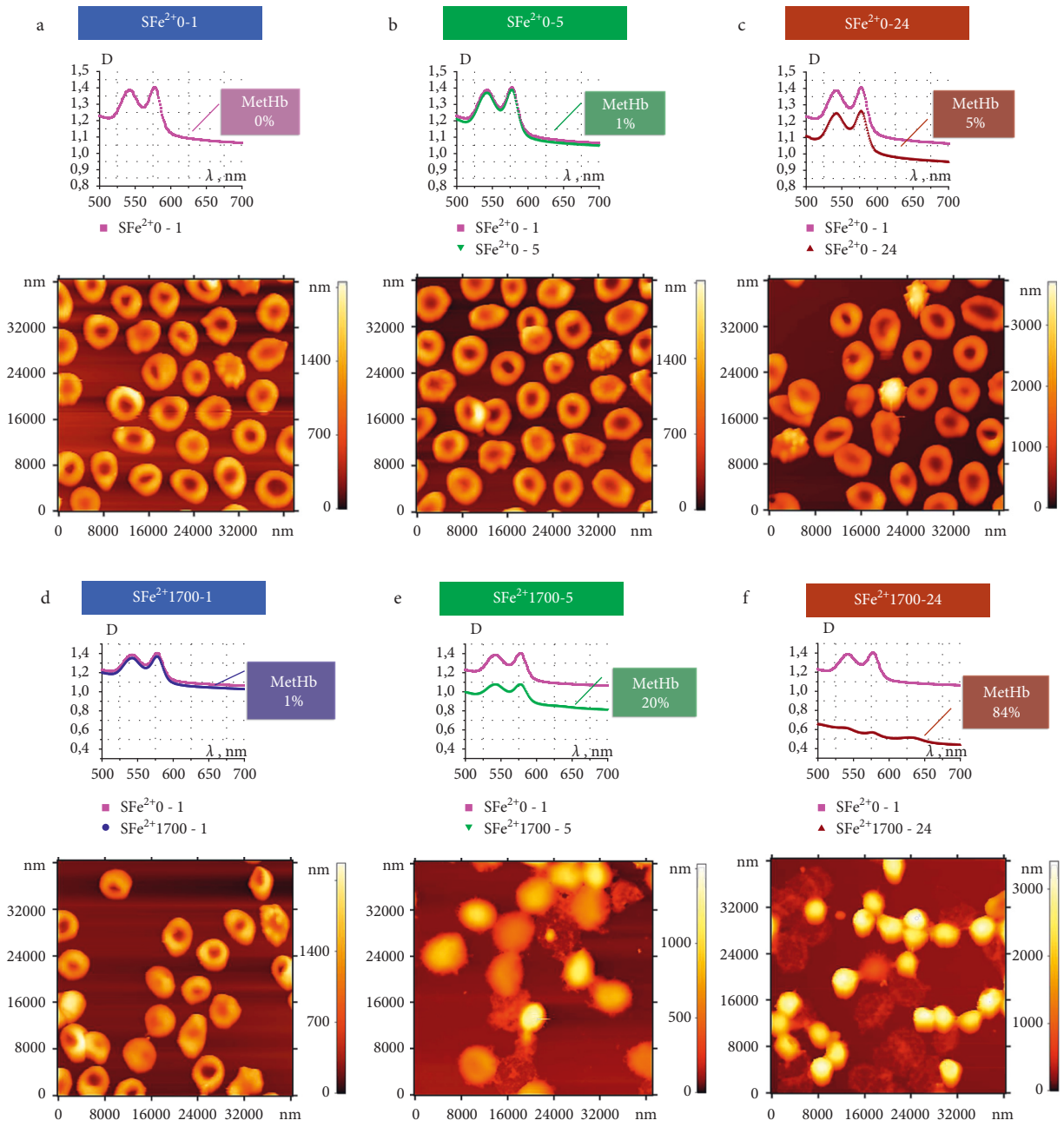


FIGURE 3: Effects of free $Fe^{2+}$ on the increase in MetHb content and the increase in polymorphisms. (a–c) Optical spectra and AFM images for the pRBC suspension ($SFe^{2+}$ 0), scale $40 \times 40\ \mu m^2$. Incubation times were 1 h (a), 5 h (b), and 24 h (c). Color scales of heights are shown for the images. The $C_{MetHb}(t)$ is indicated on each graph. (d–f) Optical spectra and AFM images for the pRBC suspension after exposure to $Fe^{2+}$ ($SFe^{2+}$ 1700), scale $40 \times 40\ \mu m^2$. Incubation times were 1 h (d), 5 h (e), and 24 h (f). The $C_{MetHb}(t)$ is indicated on each graph. Color scales of heights are shown for the images.

width ranged from 400 to 700 nm, and the length ranged from 20 to 200 nm. Some examples of bridges and chains are shown in Figure 5(b). Figure 5(c) shows the moment of chain formation from two microspherocytes, between which there is a spherocyte in the process of hemolysis, and bridges are formed between these three cells. Up to 10–12 cells were observed in chains. 30–40 cells formed clots. We observed these phenomena precisely after $Fe^{2+}$ exposure for $t_{inc}$ = 24 hours. The bridges were absent in the control and were practically not observed for $t_{inc}$ = 60 min. The formation of such structures by free iron may increase the probability of blood clot forming in blood vessels.

The structure of aggregates in such clots was different from that of aggregates in the form of coin columns from control cells. We have already observed similar aggregate clots in the case of exposure of blood to carbon monoxide [53, 60] as well as zinc ions [61]. Perhaps, this effect is associated with a change in the ratio of hemoglobin derivatives or with partial local hemolysis. In the scientific

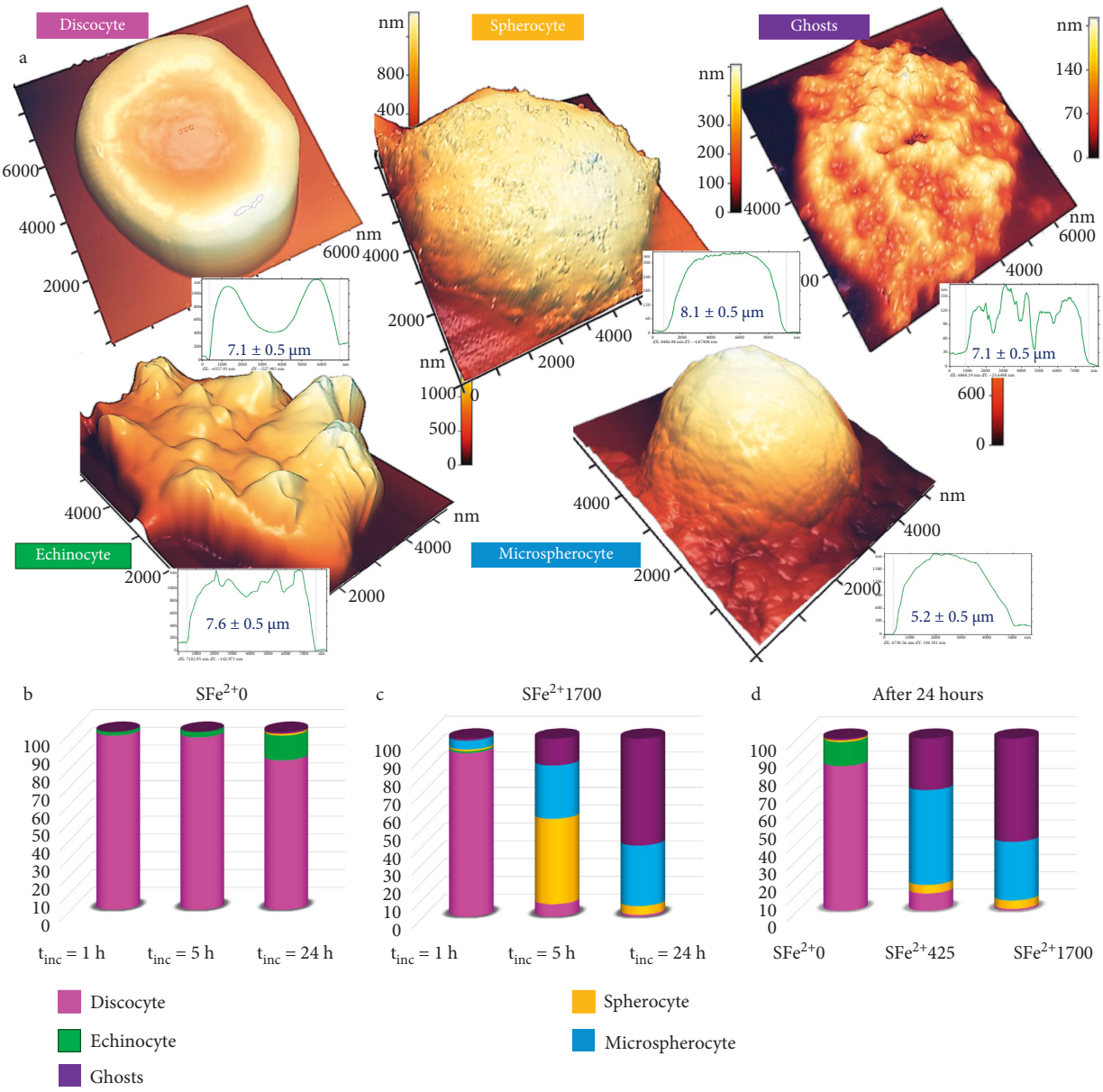


Figure 4: Typical forms of pRBCs after free $Fe^{2+}$ exposure. (a) 3D AFM images of typical cell shapes after exposure of pRBCs to free $Fe^{2+}$; color scales of cell heights are shown. On the right of each cell, the profile and its size are shown as the mean ± SD. (b, c) Histograms of the dynamics of changes in the percentage of each cell form for $SFe^{2+}$ 0 and $SFe^{2+}$ 1700, $t_{inc}$ = 1, 5, and 24 (h). On the right is the color coding for the different cell shapes. (d) Histogram of the dynamics of changes in the percentage of each cell form after 24 hours for different concentrations of free iron. On the right is the color coding for the different cell shapes.

literature, two alternative mechanisms of RBC aggregation have been conceived, namely a bridging model [62] and a local osmotic gradient model [63]. Based on the bridge model, large macromolecules are adsorbed on the cell surface and thereby connect two adjacent cells. When these bridges exceed disaggregation forces such as electrostatic repulsion, membrane deformation and mechanical shear, aggregation occurs [64]. These mechanisms may manifest themselves in the case of the action of excess iron on RBCs. Like agglutination, the phenomenon we observed is dangerous due to an increase in the formation of blood clots in vessels of various diameters.

*3.5. The pRBC Membrane Stiffness Was Increased.* In our experiments, morphological changes and the formation of MetHb were accompanied by an increase in pRBC membrane stiffness as a result of free $Fe^{2+}$ exposure of the blood. AFS was used to investigate the deep bending of pRBC membranes up to $h$ = 1000–1300 nm under the action of a probe (Figure 6(a)). Typical force curves for the control and experimental samples for $t_{inc}$ = 24 hours are shown in Figure 6(a).

The force curve for the cell membrane after exposure to $F_{Fe^{2+}1700}(h)$ is sharper than that for the control cell $F_{Fe^{2+}0}(h)$ (Figure 6(a)). The 100 measured force curves were calculated using the Hertz formula, and histograms of Young's modulus for membranes of these groups were plotted (Figure 6(b)).

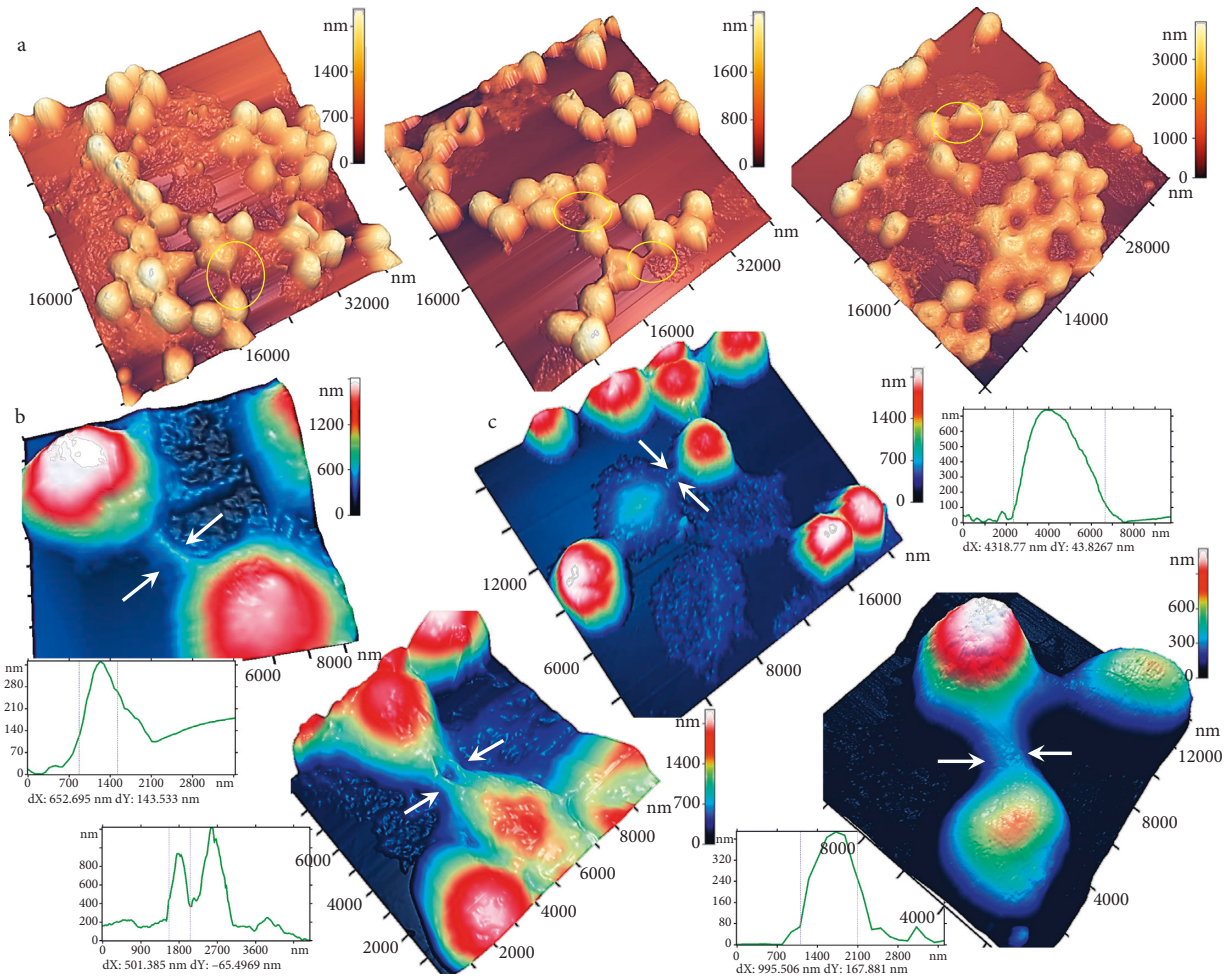


FIGURE 5: Formation of bridges, chains, and clots of pRBCs. (a) 3D AFM images of pRBCs after free $Fe^{2+}$ exposure. A color scale of heights is given for all images. Yellow circles show the areas of formation of bridges and chains. (b) 3D AFM images of typical bridges between cells and their profiles. A color scale of heights is given for all images. White arrows indicate the boundaries of the profiles. (c) Formation of a chain of two microspherocytes, between which there is a spherocyte in the process of hemolysis. Color scales of heights are shown. White arrows indicate the boundaries of the reduced profile.

The corresponding mean and variances were calculated: $E_{Fe^{2+}0} = 11 \pm 4$ kPa and $E_{Fe^{2+}1700} = 17 \pm 5$ kPa for $t_{inc} = 1$ h and $E_{Fe^{2+}0} = 15 \pm 5$ kPa and $E_{Fe^{2+}1700} = 23 \pm 8$ kPa for $t_{inc} = 24$ h. Figure 6(c) shows the distribution functions of Young's modulus for $t_{inc} = 1$ h and for $t_{inc} = 24$ h, corresponding to the study and control groups. Based on these curves, it was found that after $t_{inc} = 1$ h after exposure to $Fe^{2+}$ 1700 $\mu$M, 35% of pRBC membranes had Young's modulus values that were beyond the control values (at a level of 0.95). The results were almost the same after $t_{inc} = 24$ h, 37%. These results indicate that almost one-third of the cells had increased stiffness, which reduced their deformability and potentially caused microcirculation disorders. Earlier studies showed that the reason for the change in the stiffness of RBC membranes with an increase in oxidative processes is a change in the structure of the cytoskeleton of cells [46, 52, 58, 65–67].

*3.6. Kinetic Model of Changes in Hemoglobin Derivative Concentrations.* The biomarker for the development of oxidative processes in RBC suspensions under the influence of various physicochemical factors is the MetHb level [52, 54]. To describe the change in the MetHb level under the action of free iron, we proposed a mathematical model based on kinetic equations. The kinetic model is derived from fundamental principles as mass balance considering a constant volume and describes interactions between network components and the processes they undergo. A first-order ordinary differential equation (ODE) based on the law of mass action stating that the rate of the chemical reaction is directly proportional to the product of the reactants allowed us to describe the kinetics of the processes.

*3.6.1. Model Assumptions.* The following assumptions were made that define the model's validity range:

(1) The initial main triggering reaction for subsequent processes is the reaction of the interaction of iron ions $Fe^{2+}$ with ROS, namely, with peroxide $H_2O_2$:

$$Fe^{2+} + H_2O_2 \longrightarrow OH^{\cdot} + OH^{-} + Fe^{3+} \quad (3)$$

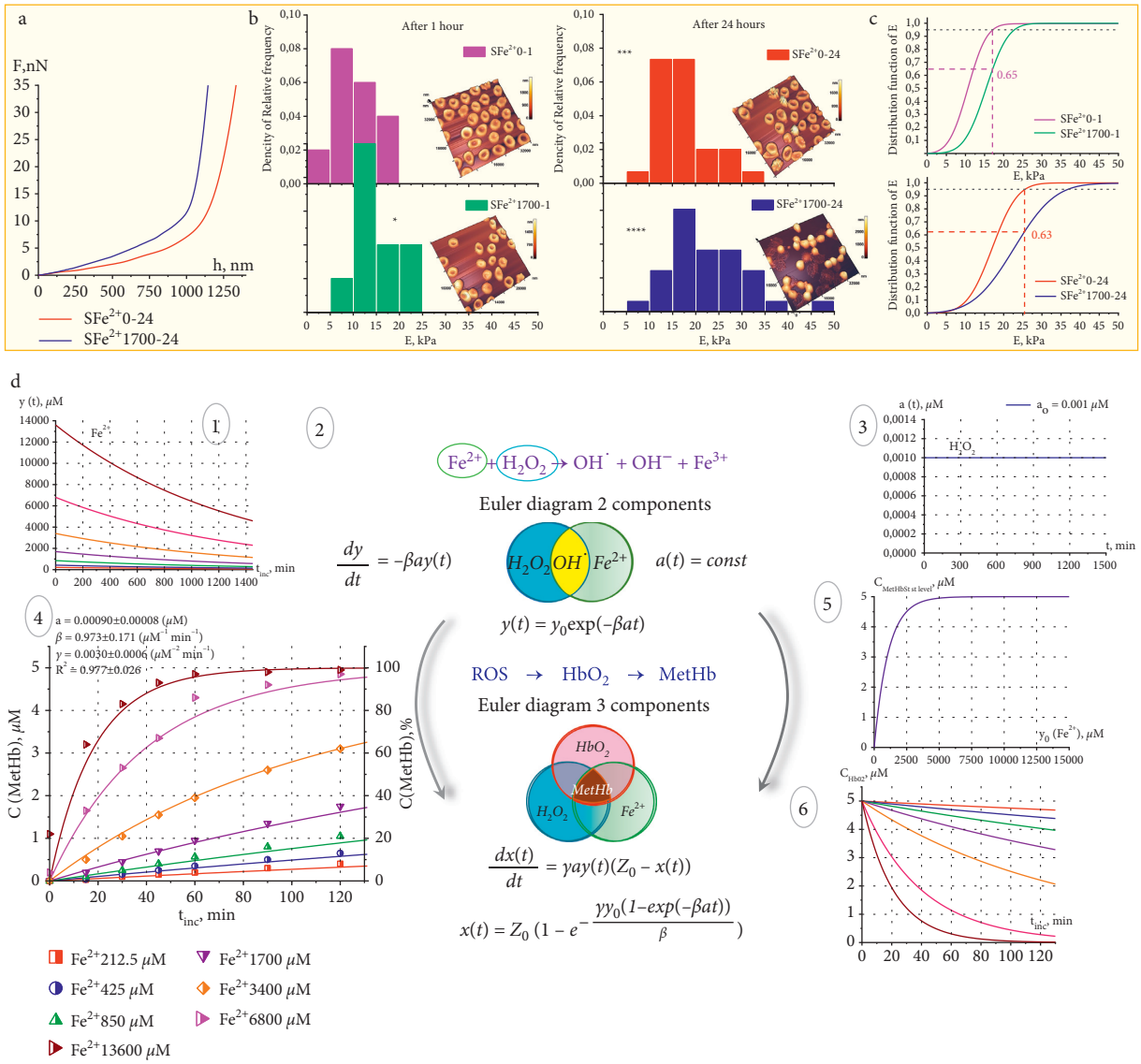


FIGURE 6: Increasing the pRBC membrane stiffness and a kinetic model. (a) Typical force curves for the control ($SFe^{2+}$ 0–24) and experimental samples ($SFe^{2+}$ 1700–24). (b) Histograms of the relative frequency density for Young's moduli of native pRBC membranes, $n = 100$ points for each histogram. For each histogram, the corresponding AFM images of pRBCs are shown. The bottom scale is the same as the top one; from 0 to 0.1 with step 0.02. The one-way ANOVA test followed by the Tukey post hoc test was used: $^{*}\,p < 0.05$, $^{***}\,p < 0.001$, and $^{****}\,p < 0.0001$ compared to $SFe^{2+}$ 0–1. (c) Distribution functions $F(E)$ for $SFe^{2+}$ 0 and $SFe^{2+}$ 1700 after 1 and 24 hours. The 0.95 level is shown as a black dashed line. (d) Kinetic model of changes in MetHb content. 1: graph $y(t)$ during the interaction of $Fe^{2+}$ ions with peroxide at constant concentration of $H_2O_2$; 2: model equations; 3: graph $a(t)$ over time (quasi-steady state condition); 4: increase in the $C_{MetHb}(t)$ in the range of incubation time $t_{inc} = 0$–120 min (symbols indicate experimental data and lines correspond the fitting functions according to calculated parameters); fitting curves were calculated according model, equation (10); 5: the dependence of steady state level of MetHb content on initial concentration $C_{Fe^{2+}}$: $C_{MetHb}(C_{Fe^{2+}})$, equation (11); 6: graph of the $C_{HbO_2}(t)$ decrease.

[9, 31, 47, 48]. During the subsequent redox reactions, the conversion of $HbO_2$ to MetHb occurs.

(2) We consider steady-state condition with respect to $C_{H_2O_2}$. The concentration of $H_2O_2$ in the system is maintained constant, $C_{H_2O_2}$ = const. The concentrations of peroxide in the blood and, accordingly, in the working solution are very low. However, it should be taken into account that in the course of subsequent ROS reactions, $H_2O_2$ is formed again [68, 69].

### 3.6.2. Two-Component Kinetic Model: The Interaction of Free $Fe^{2+}$ with $H_2O_2$

*Derivation of a Differential Equation and its Solution.* We suggest the kinetic model describing the interaction of free $Fe^{2+}$ with $H_2O_2$ in (equation (3)).

Let us denote

$y(t) = C_{Fe^{2+}}(t)$; $(dy/dt)$ is the rate of change in the concentration of iron ions $Fe^{2+}$; $\beta$ is the rate constant; and $a = C_{H_2O_2}$ = const.

We rely on the fact that the rate of the chemical reaction (equation (3)) is directly proportional to the product of the reactant concentrations, and then the ODE is as follows:

$$\frac{dy}{dt} = -\beta a y(t). \tag{4}$$

Initial condition is

$$\begin{aligned} &\text{at } t = 0, \\ &y = y_0. \end{aligned} \tag{5}$$

Solving the differential equation (equation (4)) by the method of separation of variables and taking into account the initial conditions (equation (5)), we get the dependence of the $Fe^{2+}$ change on time:

$$y(t) = y_0 \exp(-\beta a t). \tag{6}$$

Figure 6(d), 1 shows the graphs of the decrease in the concentration of iron ions $y(t)$ during their interaction with peroxide for a constant concentration $C_{H_2O_2} = 1\,\text{nM}$ (Figure 6(d), 3), which was in our experiments.

For illustration, an Euler diagram for the two-component reaction (green, $Fe^{2+}$ ions and blue, $H_2O_2$ molecules) is presented in Figure 6(d), 2. The intersection area is highlighted in yellow and corresponds to the reaction product hydroxyl radical $OH^{\cdot}$.

*3.6.3. Three-Component Model: Interaction of Free $Fe^{2+}$, $H_2O_2$, and $HbO_2$ in the Lysate. Derivation of a Differential Equation and Its Solution.* $H_2O_2$ is a long-lived representative of ROS that can diffuse over long distances. However, at the same time, it has a lower reactivity in comparison with the rest of the ROS which are short-lived and diffuse over short distances but exhibit high reactivity. As a result of the reaction (equation (3)), a hydroxyl radical $OH^{\cdot}$ is formed, which is highly reactive and short-lived. It is the hydroxyl radical that triggers and participates in subsequent redox reactions. The radical $OH^{\cdot}$ will be able to enter into further reactions with other closely located ROS and $HbO_2$.

Let us denote

$$x(t) = C_{\text{MetHb}}(t). \tag{7}$$

$Z_0$ is the initial concentration of $HbO_2$; under the experimental conditions $Z_0 = 5 \pm 0.5\,\mu\text{M}$ and $(Z_0 - x(t))$ is the concentration of $HbO_2$ at any time.

According to the mass action law, the rate of the chemical reaction is directly proportional to the product of the reactant concentrations:

$$\frac{dx(t)}{dt} = \gamma a y(t)(Z_0 - x(t)), \tag{8a}$$

where $\gamma$ is the rate constant.

Initial condition: we assume that the initial level of MetHb at $t = 0$ is

$$x_0 = 0. \tag{8b}$$

Taking into account the dependence equation (6), we write down the ODE (8a) in the form

$$\frac{dx(t)}{dt} = \gamma a y_0 (Z_0 - x(t)) \exp(-\beta a t). \tag{9a}$$

This is the first-order ODE. It is solved by the method of separation of variables:

$$\int \frac{dx}{Z_0 - x} = \int \gamma a y_0 \exp(-\beta a t)\text{dt}, \tag{9b}$$

$$\ln(Z_0 - x) = -\frac{\gamma y_0 \exp(-\beta a t)}{\beta} + B, \tag{9c}$$

where B is the arbitrary constant.

Taking into account the initial condition equation (8b), we can find that

$$B = \ln Z_0 + \frac{\gamma y_0}{\beta}. \tag{9d}$$

Substituting equation (9d) into equation (9c), we get the dependence of MetHb concentration change:

$$x(t) = Z_0\left(1 - e^{-\left(\gamma y_0 (1 - \exp(-\beta a t))/\beta\right)}\right). \tag{10}$$

The steady state level of MetHb can be found depending on the initial concentration of $Fe^{2+}$ ions $(y_0)$.

In this case, in equation (10), $t \longrightarrow \infty$. Then,

$$x(t)_{\text{stst level}} = Z_0\left(1 - e^{-\left(\gamma y_0/\beta\right)}\right). \tag{11}$$

The units of reactant concentrations are $Z_0(\mu M), x(\mu M), y_0(\mu M)$, and $a(\mu M)$; the units of parameters are $\beta(\mu M^{-1}\text{min}^{-1})$ and $\gamma(\mu M^{-2}\text{min}^{-1})$; and the time is $t$ (min).

For illustration, an Euler diagram for the 3-component reaction (red: $HbO_2$ molecules) is presented in Figure 6, 2. The intersection area is highlighted in brown and corresponds to the final reaction product MetHb.

*3.6.4. Fitting of Experimental Data.* Nonlinear curve fitting of the experimental data of the MetHb concentration change (Figures 2(b) and 2(e)) was performed according to equation (10) by using Origin Pro 2019. The unknown values of concentration $a$ and rate constants $\beta$ and $\gamma$ were considered as model parameters which describe the experimental data in the best way. The known values were $x(t)$ and $y_0$. The criterion for the optimal fitting was that the theoretical values of $x_{\text{theor}}(t)$ fit best the experimental data $x_{\text{exper}}(t)$, at a level $R^2 > 0.96$. As a result of the fitting, the values of $a$, $\beta$, and $\gamma$ were obtained for each curve corresponding to a different initial iron level $y_0$. Taking into account the data averaging, we obtained that $a = 0.00090 \pm 0.00008$ $(\mu M)$, $\beta = 0.973 \pm 0.171$ $(\mu M^{-1}\text{min}^{-1})$, $\gamma = 0.0030 \pm 0.0006$ $(\mu M^{-2}\text{min}^{-1})$, and $R^2 = 0.977 \pm 0.026$.

It is noteworthy that the theoretically found concentration of $a(C_{H_2O_2})$, which was in the equations as quasi-steady state condition, coincided with the experimental value with an

accuracy of 5–10%. This also indicates the adequacy of the model and, accordingly, the mechanism of the kinetics of the interaction of $H_2O_2$, $Fe^{2+}$, and $HbO_2$.

Figure 6(d), 4 shows lines according to dependence (equation (10)) for different initial concentrations of $Fe^{2+}$ ions which fit the experimental data (indicated by symbols) from Figure 2(d) in the first $t_{inc} = 120$ min. The steady state level of the MetHb content (saturation) and the time to reach it (or the rate) depend on the initial concentration of $Fe^{2+}$ according to equation (11) (Figure 6(d), 5). With an increment in the initial $C_{Fe^{2+}}$, the steady state level of MetHb increases in good agreement with the experimental data (Figure 2(d)). This is the confirmation of the adequacy of the model.

The increase in MetHb was accompanied by a decrease in $HbO_2$ (Figure 6(d), 6). At a high initial concentration of $C_{Fe^{2+}} = 6800–13600\ \mu M$, the rate of the Fenton reaction and, accordingly, the rate of decrease in $HbO_2$ will be large, and accordingly, for a short incubation time of 100–200 min, almost all $HbO_2$ will be converted to MetHb (Figure 6(d), 6). The reason for the steady state of the MetHb level in this case is the use of all $HbO_2$ molecules during this time of observation. In another situation, with a low initial concentration of iron, the rate of MetHb formation will be insignificant. In this case, a steady state of MetHb concentration will be observed but already at a lower level. The reason for the steady state will be already an insufficient amount of iron ions decreasing with the time.

*3.7. RBCs as a Key Link in the Influence of Free Iron Overload: The Scheme Representation.* Despite the publication of numerous studies concerning the problems of iron overload, the comprehensive study of excess iron influence on RBCs remains limited. To better identify the processes in RBCs under iron overload, we used biophysical methods to perform a modeling study *in vitro*.

In a healthy organism, there is a dynamic balance of concentrations of $Fe^{2+}/Fe^{3+}$, $H_2O_2$ /ROS, and $HbO_2$/MetHb. Normally, the iron balance is maintained by iron transport proteins [1]. Free iron overload occurs in a number of diseases (Figure 7 (a)). In critically ill patients, particularly in cases of sepsis, the capacity to detoxify cell-free hemoglobin is reduced [16, 18]. As a result, the equilibrium is disturbed, and the system goes into another state, while collective disproportions arise in all elements of the system in one way or another (Figure 7 (b)).

In this chain of pathological process development, RBCs play a key role (Figure 7 (b) 1–6). Excess iron accumulation causes distortions through the production of ROS [2] via the Fenton reaction (Figure 7 (b1) and (b2)), with the generation of toxic hydroxyl $OH^{\cdot}$ radicals, which are highly reactive and toxic [70]. The generation of ROS (Figure 7 (b3)) leads to the peroxidation of membrane lipids and cellular proteins, resulting in membrane and cytoskeleton distortions and hemoglobin derivative transformations (Figure 7 (b4)). As has already been noted repeatedly, RBC hemolysis is a dangerous consequence of the action of free iron on the blood. When $OH^{\bullet}$ interacts with membrane lipids, chain reactions of lipid peroxidation occur (Figure 7 (b4)). As a result, the hydrophilicity of bonds in lipid tails increases locally, and local hydraulic pores are formed. This leads to disruption of the ionic balance in RBCs, and osmosis occurs. This leads to a change in cell morphology as well as partial and complete hemolysis of spherocytes.

Also, high iron condition might induce RBC surface protein denaturation, leading to their adhesion to each other. Probably with excess iron, changes in the band 3 proteins and spectrin occur (Figure 7 (b4)). This leads to change of cytoskeleton and membrane surface nanostructure. We observed similar phenomena using AFM studies of the influence of Zn ions, UV radiation, and hemin, during long-term storage of pRBCs [52, 57, 71, 72]. Clusterization of protein may be the reason of bridge and clot formation.

Serious disorders in the pRBCs due to ROS in result of iron overload are shown in Figure 7 b4 and b5, and we established those in our experiments *in vitro* (Figures 3 and 4).

The effect of $Fe^{2+}$ on RBCs occurs under conditions positive feedback in the system *free iron–blood* (Figure 7). An excess of free iron leads to the appearance of free $HbO_2$, MetHb, and to a high concentration of free hemes, which in turn leads to free iron and ROS [9, 73]. These positive feedbacks are shown in Figure 7 c, b $1^{/}$, $3^{/}$, $4^{/}$, $5^{/}$, and $6^{/}$.

Disorders in RBCs can cause abnormalities cascade of pathological processes in organisms (Figure 7 (c)) [26, 27, 37, 73–83].

RBCs may be potential sources of clinical changes *in vivo* in the cardiovascular system (Figure 7 (c)). In particular, the clinical consequence of excess iron is atherosclerosis, which increases the possibility of hemolysis of pRBCs, therefore leading to an increase in the production of free iron and oxidized products. In addition to hypoperfusion, up to a complete blockage of blood flow, massive hemolysis occurs with the appearance of free hemoglobin and the increase in the level of free iron. A vicious cycle is created when iron initiates an inflammatory process, including thrombovasculitis, and the blockade of micro- and macrocirculation creates conditions for hemolysis and an increase in the level of free heme iron in the blood serum [8, 26, 84]. As a result, a rapid increase in respiratory insufficiency occurs due to blockage of the pulmonary blood flow. Microvascular pulmonary thrombovasculitis obliterans, which is characterized by thrombosis of not only microcirculatory vessels but also larger vessels, is typical for COVID-19.

In our *in vitro* studies, we tried to answer the question what disorders can occur in RBCs which can modify their functions. We established the pattern of the simultaneous development of heterogeneous processes under the action of excess iron: changes in the morphology of pRBCs, the formation of bridges between cells, the formation of clots (such as pRBC agglutination), the formation of MetHb, and increasing of membrane Young's modulus (Figures 2–7 (b5), (b6)).

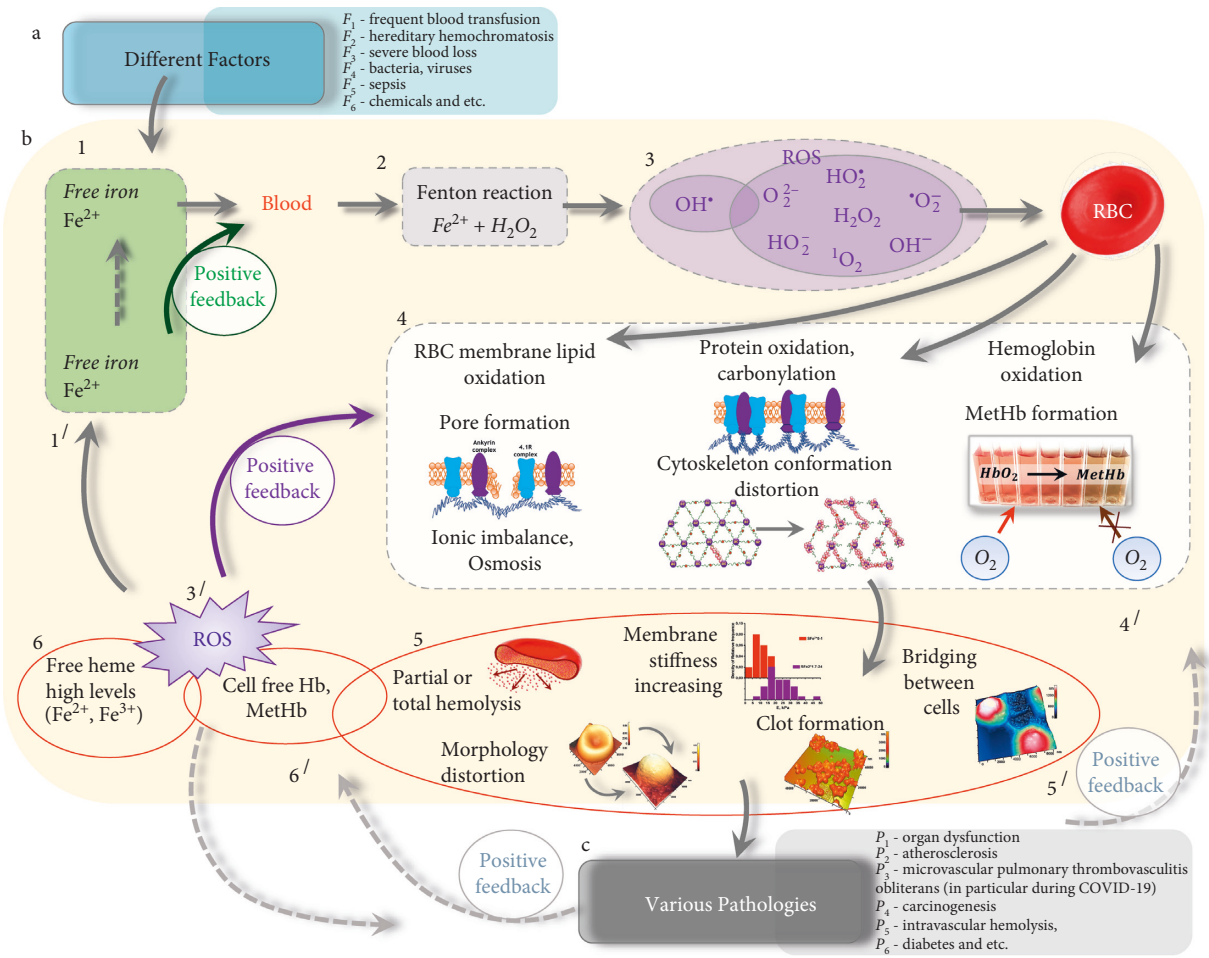


FIGURE 7: The scheme of the mechanism of the toxic action of excess iron on RBCs, possible distortions in constituent elements of cells, and possible pathophysiological consequences in the clinic. (a) Various factors $F_i$, which can serve as a source of free iron. (b) Violations in RBCs. 1, 1′: formation of free iron; 2: fenton reaction. 3, 3′: ROS formation; 4, 4′: violations in constituent elements of RBCs; 5, 5′: pathological processes in RBCs; 6, 6′: formation of cell-free Hb, free heme. (c) Various clinical consequences $P_i$. There are indicated positive feedbacks in the process development.

## 4. Conclusion

In conclusion, iron is useful and nontoxic, when bound in our bodies in optimal quantities. However, overload of free iron is dangerous and can cause powerful oxidative stress. In biophysical experiments *in vitro*, we have experimentally established a complex of changes that can occur in pRBCs and lead to the development of pathological processes. Thus, we have shown that pRBCs may be the key link in the pathology influence of free iron overload. Patterns established in our experiments *in vitro* can allow to expand the understanding of the mechanisms of the toxic adverse effect of excess free iron on the blood and the circulatory system, and, consequently, to develop adequate methods for patient treatment.

## Data Availability

The data used to support the findings of this study are available from the corresponding author upon request.

## Conflicts of Interest

The authors declare that they have no conflicts of interest relevant to this manuscript.

## Acknowledgments

This work has been supported by the Ministry of Science and Higher Education of the Russian Federation, Priority 2030.

## References

[1] T. D. Coates, "Physiology and pathophysiology of iron in hemoglobin-associated diseases," *Free Radical Biology and Medicine*, vol. 72, pp. 23–40, 2014.

[2] Y. Kohgo, K. Ikuta, T. Ohtake, Y. Torimoto, and J. Kato, "Body iron metabolism and pathophysiology of iron overload," *International Journal of Hematology*, vol. 88, no. 1, pp. 7–15, 2008.

[3] K. Leecharoenkiat, P. Lithanatudom, W. Sornjai, and D. R. Smith, "Iron dysregulation in beta-thalassemia,"

*Asian Pacific Journal of Tropical Medicine*, vol. 9, no. 11, pp. 1035–1043, 2016.

[4] A. Shander and K. Sazama, "Clinical consequences of iron overload from chronic red blood cell transfusions, its diagnosis, and its management by chelation therapy," *Transfusion*, vol. 50, no. 5, pp. 1144–1155, 2010.

[5] M. T. Gladwin and D. B. Kim-Shapiro, "Storage lesion in banked blood due to hemolysis-dependent disruption of nitric oxide homeostasis," *Current Opinion in Hematology*, vol. 16, no. 6, pp. 515–523, 2009.

[6] K. Grimshaw, J. Sahler, S. L. Spinelli, R. P. Phipps, and N. Blumberg, "New frontiers in transfusion biology: identification and significance of mediators of morbidity and mortality in stored red blood cells," *Transfusion*, vol. 51, no. 4, pp. 874–880, 2011.

[7] A. J. Ghio, J. D. Carter, J. H. Richards, L. D. Richer, C. K. Grissom, and M. R. Elstad, "Iron and iron-related proteins in the lower respiratory tract of patients with acute respiratory distress syndrome," *Critical Care Medicine*, vol. 31, no. 2, pp. 395–400, 2003.

[8] Y. P. Orlov, V. T. Dolgikh, E. I. Vereschagin et al., "Is there a connection between iron exchange and COVID-19?" *Messenger of Anesthesiology and Resuscitation*, vol. 17, no. 4, pp. 6–13, 2020.

[9] J. M. Rifkind, J. G. Mohanty, and E. Nagababu, "The pathophysiology of extracellular hemoglobin associated with enhanced oxidative reactions," *Frontiers in Physiology*, vol. 5, p. 500, 2014.

[10] C. D. Reiter, X. Wang, J. E. Tanus-Santos et al., "Cell-free hemoglobin limits nitric oxide bioavailability in sickle-cell disease," *Nature Medicine*, vol. 8, no. 12, pp. 1383–1389, 2002.

[11] C. Meyer, C. Heiss, C. Drexhage et al., "Hemodialysis-induced release of hemoglobin limits nitric oxide bioavailability and impairs vascular function," *Journal of the American College of Cardiology*, vol. 55, no. 5, pp. 454–459, 2010.

[12] F. T. Billings 4th, S. K. Ball, L. J. Roberts 2nd, and M. Pretorius, "Postoperative acute kidney injury is associated with hemoglobinemia and an enhanced oxidative stress response," *Free Radical Biology and Medicine*, vol. 50, no. 11, pp. 1480–1487, 2011.

[13] E. L. Brittain, D. R. Janz, E. D. Austin et al., "Elevation of plasma cell-free hemoglobin in pulmonary arterial hypertension," *Chest*, vol. 146, no. 6, pp. 1478–1485, 2014.

[14] K. Inthawong, P. Charoenkwan, S. Silvilairat et al., "Pulmonary hypertension in non-transfusion-dependent thalassemia: correlation with clinical parameters, liver iron concentration, and non-transferrin-bound iron," *Hematology*, vol. 20, no. 10, pp. 610–617, 2015.

[15] M. Adamzik, T. Hamburger, F. Petrat, J. Peters, H. de Groot, and M. Hartmann, "Free hemoglobin concentration in severe sepsis: methods of measurement and prediction of outcome," *Critical Care (London, England)*, vol. 16, no. 4, Article ID R125, 2012.

[16] D. R. Janz, J. A. Bastarache, J. F. Peterson et al., "Association between cell-free hemoglobin, acetaminophen, and mortality in patients with sepsis: an observational study," *Critical Care Medicine*, vol. 41, no. 3, pp. 784–790, 2013.

[17] D. R. Janz, J. A. Bastarache, T. W. Rice et al., "Randomized, placebo-controlled trial of acetaminophen for the reduction of oxidative injury in severe sepsis: the acetaminophen for the reduction of oxidative injury in severe sepsis trial," *Critical Care Medicine*, vol. 43, no. 3, pp. 534–541, 2015.

[18] D. R. Janz and L. B. Ware, "The role of red blood cells and cell-free hemoglobin in the pathogenesis of ARDS," *Journal of Intensive Care*, vol. 3, no. 1, p. 20, 2015.

[19] T. Ganz and E. Nemeth, "Iron metabolism: interactions with normal and disordered erythropoiesis," *Cold Spring Harbor Perspectives in Medicine*, vol. 2, no. 5, Article ID a011668, 2012.

[20] K. D. Poss and S. Tonegawa, "Heme oxygenase 1 is required for mammalian iron reutilization," *Proceedings of the National Academy of Sciences*, vol. 94, no. 20, pp. 10919–10924, 1997.

[21] K. M. Utzschneider and K. V. Kowdley, "Hereditary hemochromatosis and diabetes mellitus: implications for clinical practice," *Nature Reviews Endocrinology*, vol. 6, no. 1, pp. 26–33, 2010.

[22] V. R. Gordeuk, J. R. Delanghe, M. R. Langlois, and J. R. Boelaert, "Iron status and the outcome of HIV infection: an overview," *Journal of Clinical Virology*, vol. 20, no. 3, pp. 111–115, 2001.

[23] S. Nekhai, N. Kumari, and S. Dhawan, "Role of cellular iron and oxygen in the regulation of HIV-1 infection," *Future Virology*, vol. 8, no. 3, pp. 301–311, 2013.

[24] M. Thursz, "Iron, haemochromatosis and thalassaemia as risk factors for fibrosis in hepatitis C virus infection," *Gut*, vol. 56, no. 5, pp. 613-614, 2007.

[25] D.-M. Zou and W.-L. Sun, "Relationship between hepatitis C virus infection and iron overload," *Chinese Medical Journal*, vol. 130, no. 7, pp. 866–871, 2017.

[26] A. Cavezzi, E. Troiani, and S. Corrao, "COVID-19: hemoglobin, iron, and hypoxia beyond inflammation. A narrative review." *Clinics and Practice*, vol. 10, no. 2, p. 1271, 2020.

[27] B. B. Muhoberac, "What can cellular redox, iron, and reactive oxygen species suggest about the mechanisms and potential therapy of COVID-19?" *Frontiers in Cellular and Infection Microbiology*, vol. 10, Article ID 569709, 2020.

[28] R. Biary, L. Li, and R. S. Hoffman, "Intravenous iron overdose: treat the patient not the number," *Toxicology Communications*, vol. 3, no. 1, pp. 37–39, 2019.

[29] D. Yu and M. A. Giffen, "Suicidal iron overdose: a case report and review of literature," *Journal of Forensic Sciences*, vol. 66, no. 4, pp. 1564–1569, 2021.

[30] A. S. Manoguerra, A. R. Erdman, L. L. Booze et al., "Iron ingestion: an evidence-based consensus guideline for out-of-hospital management," *Clinical Toxicology*, vol. 43, no. 6, pp. 553–570, 2005.

[31] A. Cornelissen, L. Guo, A. Sakamoto, R. Virmani, and A. V. Finn, "New insights into the role of iron in inflammation and atherosclerosis," *EBioMedicine*, vol. 47, pp. 598–606, 2019.

[32] S. Kiechl, F. Aichner, F. Gerstenbrand et al., "Body iron stores and presence of carotid atherosclerosis. Results from the bruneck Study," *Arteriosclerosis and Thrombosis: A Journal of Vascular Biology*, vol. 14, no. 10, pp. 1625–1630, 1994.

[33] P. Syrovatka, P. Kraml, K. Hulikova et al., "Iron stores are associated with asymptomatic atherosclerosis in healthy men of primary prevention," *European Journal of Clinical Investigation*, vol. 41, no. 8, pp. 846–853, 2011.

[34] T.-P. Tuomainen, K. Kontula, K. Nyyssönen, T. A. Lakka, T. Heliö, and J. T. Salonen, "Increased risk of acute myocardial infarction in carriers of the hemochromatosis gene Cys282Tyr mutation: a prospective cohort study in men in eastern Finland," *Circulation*, vol. 100, no. 12, pp. 1274–1279, 1999.

[35] T.-P. Tuomainen, K. Punnonen, K. Nyyssönen, and J. T. Salonen, "Association between body iron stores and the risk of acute myocardial infarction in men," *Circulation*, vol. 97, no. 15, pp. 1461–1466, 1998.

[36] E. Pretorius, "The adaptability of red blood cells," *Cardiovascular Diabetology*, vol. 12, no. 1, p. 63, 2013.

[37] T. D. Coates and J. C. Wood, "How we manage iron overload in sickle cell patients," *British Journal of Haematology*, vol. 177, no. 5, pp. 703–716, 2017.

[38] P. I. Fianza, A. Rahmawati, S. H. Widihastha et al., "Iron overload in transfusion-dependent Indonesian thalassemic patients," *Anemia.*vol. 2021, Article ID 5581831, 8 pages, 2021.

[39] C. P. Ozment and J. L. Turi, "Iron overload following red blood cell transfusion and its impact on disease severity," *Biochimica et Biophysica Acta*, vol. 1790, no. 7, pp. 694–701, 2009.

[40] S. Sahu, Hemlata, and A. Verma, "Adverse events related to blood transfusion," *Indian Journal of Anaesthesia*, vol. 58, no. 5, pp. 543–551, 2014.

[41] R. I. Litvinov and J. W. Weisel, "Role of red blood cells in haemostasis and thrombosis," *ISBT Science Series*, vol. 12, no. 1, pp. 176–183, 2017.

[42] E. Pretorius, N. Vermeulen, J. Bester, J. L. du Plooy, and G. S. Gericke, "The effect of iron overload on red blood cell morphology," *The Lancet*, vol. 383, no. 9918, p. 722, 2014.

[43] A. Banerjee, T. Dey, A. K. Ghosh, S. Mishra, D. Bandyopadhyay, and A. Chattopadhyay, "Insights into the ameliorative effect of oleic acid in rejuvenating phenylhydrazine induced oxidative stress mediated morpho-functionally dismantled erythrocytes," *Toxicology Reports*, vol. 7, pp. 1551–1563, 2020.

[44] E. Kozlova, A. Chernysh, E. Manchenko, V. Sergunova, and V. Moroz, "Nonlinear biomechanical characteristics of deep deformation of native RBC membranes in normal state and under modifier action," *Scanning*, vol. 2018, Article ID 1810585, 13 pages, 2018.

[45] F. S. Ruggeri, C. Marcott, S. Dinarelli et al., "Identification of oxidative stress in red blood cells with nanoscale chemical resolution by infrared nanospectroscopy," *International Journal of Molecular Sciences*, vol. 19, no. 9, 2018.

[46] E. Sherstyukova, A. Chernysh, V. Moroz, E. Kozlova, V. Sergunova, and O. Gudkova, "The relationship of membrane stiffness, cytoskeleton structure and storage time of pRBCs," *Vox Sanguinis*, vol. 116, no. 4, pp. 405–415, 2021.

[47] E. L. MacKenzie, K. Iwasaki, and Y. Tsuji, "Intracellular iron transport and storage: from molecular mechanisms to health implications," *Antioxidants & Redox Signaling*, vol. 10, no. 6, pp. 997–1030, 2008.

[48] S. M. Sadrzadeh, E. Graf, S. S. Panter, P. E. Hallaway, and J. W. Eaton, "Hemoglobin. A biologic fenton reagent," *Journal of Biological Chemistry*, vol. 259, no. 23, pp. 14354–14356, 1984.

[49] S. Stohs and D. Bagchi, "Oxidative mechanisms in the toxicity of metal ions," *Free Radical Biology and Medicine*, vol. 18, no. 2, pp. 321–336, 1995.

[50] L. Bellavia, J. F. DuMond, A. Perlegas, S. Bruce King, and D. B. Kim-Shapiro, "Nitroxyl accelerates the oxidation of oxyhemoglobin by nitrite," *Nitric Oxide*, vol. 31, pp. 38–47, 2013.

[51] R. D. Sharma, G. D. Katkar, M. S. Sundaram et al., "Oxidative stress-induced methemoglobinemia is the silent killer during snakebite: a novel and strategic neutralization by melatonin," *Journal of Pineal Research*, vol. 59, no. 2, pp. 240–254, 2015.

[52] E. Kozlova, A. Chernysh, V. Sergunova, O. Gudkova, E. Manchenko, and A. Kozlov, "Atomic force microscopy study of red blood cell membrane nanostructure during oxidation-reduction processes," *Journal of molecular recognition: JMR*, vol. 31, no. 10, Article ID e2724, 2018.

[53] E. Kozlova, A. Chernysh, A. Kozlov, V. Sergunova, and E. Sherstyukova, "Assessment of carboxyhemoglobin content in the blood with high accuracy: wavelength range optimization for nonlinear curve fitting of optical spectra," *Heliyon*, vol. 6, no. 8, Article ID e04622, 2020.

[54] E Kozlova, A Chernysh, V. Moroz, V. Sergunova, A Zavialova, and A Kuzovlev, "Nanoparticles of perfluorocarbon emulsion contribute to the reduction of methemoglobin to oxyhemoglobin," *International Journal of Pharmaceutics*, vol. 497, no. 1–2, pp. 88–95, 2016.

[55] A. V. Buys, M.-J. Van Rooy, P. Soma, D. Van Papendorp, B. Lipinski, and E. Pretorius, "Changes in red blood cell membrane structure in type 2 diabetes: a scanning electron and atomic force microscopy study," *Cardiovascular Diabetology*, vol. 12, no. 1, p. 25, 2013.

[56] E. Kozlova, A. Chernysh, V. Moroz, V. Sergunova, O. Gudkova, and E. Manchenko, "Morphology, membrane nanostructure and stiffness for quality assessment of packed red blood cells," *Scientific Reports*, vol. 7, no. 1, p. 7846, 2017.

[57] E. Kozlova, A. Chernysh, V. Moroz et al., "Two-step process of cytoskeletal structural damage during long-term storage of packed red blood cells," *Blood Transfus*, vol. 19, no. 2, pp. 124–134, 2021.

[58] A. Sinha, T. T. T. Chu, M. Dao, and R. Chandramohanadas, "Single-cell evaluation of red blood cell bio-mechanical and nano-structural alterations upon chemically induced oxidative stress," *Scientific Reports*, vol. 5, no. 1, p. 9768, 2015.

[59] A. R. Díaz-Marrero, M. C. Rodríguez González, A. Hernández Creus, A. Rodríguez Hernández, and J. J. Fernández, "Damages at the nanoscale on red blood cells promoted by fire corals," *Scientific Reports*, vol. 9, no. 1, Article ID 14298, 2019.

[60] E. K. Kozlova, V. A. Sergunova, A. P. Kozlov, E. A. Sherstyukova, and O. E. Gudkova, "Changes in the morphology of erythrocytes after in vitro exposure of blood to carbon monoxide," *Almanac of Clinical Medicine*, vol. 47, no. 7, pp. 669–678, 2019.

[61] A. M. Chernysh, E. K. Kozlova, V. V. Moroz, V. A. Sergunova, O. Y. Gudkova, and M. S. Fedorova, "Reversible zinc-induced injuries to erythrocyte membrane nanostructure," *Bulletin of Experimental Biology and Medicine*, vol. 154, no. 1, pp. 84–88, 2012.

[62] V. X. Du, D. Huskens, C. Maas, R. Al Dieri, P. G. de Groot, and B. de Laat, "New insights into the role of erythrocytes in thrombus formation," *Seminars in Thrombosis and Hemostasis*, vol. 40, no. 1, pp. 72–80, 2014.

[63] O. K. Baskurt and H. J. Meiselman, "Erythrocyte aggregation: basic aspects and clinical importance," *Clinical Hemorheology and Microcirculation*, vol. 53, no. 1–2, pp. 23–37, 2013.

[64] S. Chien and L. A. Sung, "Physicochemical basis and clinical implications of red cell aggregation," *Clinical Hemorheology and Microcirculation*, vol. 7, pp. 71–91, 1987.

[65] V. A. Sergunova, O. E. Gudkova, E. A. Manchenko et al., "The effect of the erythrocyte suspension temperature on the morphology and nanostructure of cell membranes," *General Reanimatology*, vol. 13, no. 4, pp. 30–37, 2017.

[66] Z. Xu, Y. Zheng, X. Wang, N. Shehata, C. Wang, and Y. Sun, "Stiffness increase of red blood cells during storage," *Microsystems & Nanoengineering*, vol. 4, no. 1, Article ID 17103, 2018.

[67] B. Zhang, B. Liu, H. Zhang, and J. Wang, "Erythrocyte stiffness during morphological remodeling induced by carbon ion radiation," *PLoS One*, vol. 9, no. 11, Article ID e112624, 2014.

[68] F. Collin, "Chemical basis of reactive oxygen species reactivity and involvement in neurodegenerative diseases," *International Journal of Molecular Sciences*, vol. 20, no. 10, 2019.

[69] D. J. Schaer and P. W. Buehler, "Cell-free hemoglobin and its scavenger proteins: new disease models leading the way to targeted therapies," *Cold Spring Harbor Perspectives in Medicine*, vol. 3, no. 6, 2013.

[70] E. Gammella, S. Recalcati, and G. Cairo, "Dual role of ROS as signal and stress agents: iron tips the balance in favor of toxic effects," *Oxidative Medicine and Cellular Longevity*, vol. 2016, Article ID 8629024, 9 pages, 2016.

[71] E. Kozlova, A. Chernysh, V. Moroz, O. Gudkova, V. Sergunova, and A. Kuzovlev, "Transformation of membrane nanosurface of red blood cells under hemin action," *Scientific Reports*, vol. 4, no. 1, p. 6033, 2014.

[72] E. Kozlova, A. Chernysh, V. Moroz et al., "Opposite effects of electroporation of red blood cell membranes under the influence of zinc ions," *Acta of Bioengineering and Biomechanics*, vol. 14, no. 1, pp. 3–13, 2012.

[73] A. A. Agyemang, S. V. Kvist, N. Brinkman et al., "Cell-free oxidized hemoglobin drives reactive oxygen species production and pro-inflammation in an immature primary rat mixed glial cell culture," *Journal of Neuroinflammation*, vol. 18, no. 1, p. 42, 2021.

[74] Z. I. Cabantchik, C. Moreau, and D. Devos, "Iron chelation for diseases of regional siderosis," *Blood*, vol. 122, no. 21, p. 3435, 2013.

[75] K. Farmaki, I. Tzoumari, C. Pappa, G. Chouliaras, and V. Berdoukas, "Normalisation of total body iron load with very intensive combined chelation reverses cardiac and endocrine complications of thalassaemia major," *British Journal of Haematology*, vol. 148, no. 3, pp. 466–475, 2010.

[76] B. Lipinski and E. Pretorius, "Hydroxyl radical-modified fibrinogen as a marker of thrombosis: the role of iron," *Hematology*, vol. 17, no. 4, pp. 241–247, 2012.

[77] T. Sugiura, Y. Dohi, H. Takase, S. Fujii, Y. Seo, and N. Ohte, "Analytical evaluation of serum non-transferrin-bound iron and its relationships with oxidative stress and cardiac load in the general population," *Medicine (Baltimore)*, vol. 100, no. 7, Article ID e24722, 2021.

[78] J. D. Belcher, J. D. Beckman, G. Balla, J. Balla, and G. Vercellotti, "Heme degradation and vascular injury," *Antioxidants & Redox Signaling*, vol. 12, no. 2, pp. 233–248, 2010.

[79] C. Borgna-Pignatti, M. D. Cappellini, P. Stefano et al., "Survival and complications in thalassemia," *Annals of the New York Academy of Sciences*, vol. 1054, no. 1, pp. 40–47, 2005.

[80] Y. Ginzburg and S. Rivella, "$\beta$-thalassemia: a model for elucidating the dynamic regulation of ineffective erythropoiesis and iron metabolism," *Blood*, vol. 118, no. 16, pp. 4321–4330, 2011.

[81] M. Gram, S. Sveinsdottir, M. Cinthio et al., "Extracellular hemoglobin - mediator of inflammation and cell death in the choroid plexus following preterm intraventricular hemorrhage," *Journal of Neuroinflammation*, vol. 11, no. 1, p. 200, 2014.

[82] H. M. Habib, S. Ibrahim, A. Zaim, and W. H. Ibrahim, "The role of iron in the pathogenesis of COVID-19 and possible treatment with lactoferrin and other iron chelators," *Biomedicine & Pharmacotherapy*, vol. 136, Article ID 111228, 2021.

[83] S. Kumar and U. Bandyopadhyay, "Free heme toxicity and its detoxification systems in human," *Toxicology Letters*, vol. 157, no. 3, pp. 175–188, 2005.

[84] F. F. Dutra and M. T. Bozza, "Heme on innate immunity and inflammation," *Frontiers in Pharmacology*, vol. 5, p. 115, 2014.